JOURNAL OF MATERIALS SCIENCE **34** (1999) 59–64

The melt structures above the liquidus in SiCp/Al composite

TONGXIANG FAN, ZHONGLIANG SHI, DI ZHANG, RENJIE WU
State Key Laboratory of Metal Matrix Composites, Shanghai Jiao Tong University, Shanghai, 200030, People's Republic of China
E-mail: SKLMMC@mail.sjtu.edu.cn

The properties and the structures of liquid melt above the liquidus play an important role in determining the resultant properties of the alloy and the composite. In this paper, the melt structures of SiCp/Al composites with two different reinforcement volume fractions were investigated using liquid metal X-ray diffraction and differential scanning calorimetry. The experimental results showed that the melt structures of SiCp/Al composite are different from that of liquid matrix alloy, a Si–Si hump in the pair radial distribution function in SiCp/Al composite melt and the DSC trace indicated that Si is not well distributed above the liquidus, the size change of short-range-order (SRO) in SiCp/Al composite melt indicated the diffusion of Si from chemical reaction between SiC and molten Al is possible only after a given temperature or after some extent concentration fluctuation of Si. The mechanisms for the observed phenomenon are also discussed in this paper.

1. Introduction

Discontinuously reinforced metal matrix composites (DRMMCs) are very attractive in aerospace and automotive industries for their properties, such as high modulus, high specific stiffness, high temperature strength, low coefficient of thermal expansion, good wear resistance and good workability and isotropy. A large and increasing proportion of DRMMCs are presently produced by solidification processing, in which the metal matrix is molten before it is combined with the particles, whiskers, or fibers that are to serve as its reinforcing phase in the final composite material. Fluid flow, mass and heat transfer, chemical reaction and solidification phenomena take place in the composite material before it is fully solidified, due to the existence of reinforcing particles, the solidification processing of the metal matrix composite is different from that of the matrix alloy. The properties and the structures of liquid melt above the liquidus play an important role in determining the resultant properties of the alloy and the composite.

Recently, studies on the structure and properties of the liquid are receiving more attention and some progress has been made [1–3]. On the other hand, SiCp/Al composites are one of the most important DRMMCs and it is now established that SiC reacts with molten aluminum, producing Al_4C_3 and silicon, according to the following reaction

$$4Al + 3SiC \longrightarrow Al_4C_3 + 3Si \qquad (1)$$

Silicon formed in this reaction dissolves in unreacted aluminum, giving rise to an Al-Si liquid alloy [4–6]. The melt structures and the distribution and diffusion of silicon is responsible for the further reaction between SiC and molten aluminum above the liquidus, and, meanwhile, the knowledge of melt structure, especially the local melt structure around the reinforcement is more important, since it may control (at least partially) the following stage of the interface reaction zone, and thereby affect the final microstructures and properties of the interface. With regard to metal matrix composite, and, in particular, the particle reinforced aluminum matrix composites, very few studies have been carried out on the melt structures of composites. In this paper, the melt structures of SiCp/Al composites above the liquidus were investigated for the first time using liquid metal X-ray diffraction (LMXRD) and differential scanning calorimetry (DSC) in order to provide basic profiles of melt structure in SiCp/Al composites.

2. Experimental procedures

2.1. Composite fabrication

SiCp/pure Al composites used in this study were fabricated using vacuum-high pressure infiltration processing. The dominant phase of SiCp used as the reinforcement was α-SiC(6H) and the average size of the SiCp was $\sim$7 μm. The SiCp used in this study had not undergone any surface modification such as surface oxidation, surface coating, etc. Two types of SiCp/Al composite (10 and 40 vol %SiC) were used to vary the melt structure characteristics during the remelting.

2.2. Liquid metal X-ray diffraction

X-ray diffraction was carried out using a θ–θ type liquid metal X-ray diffractometer in the Ukraine Academy

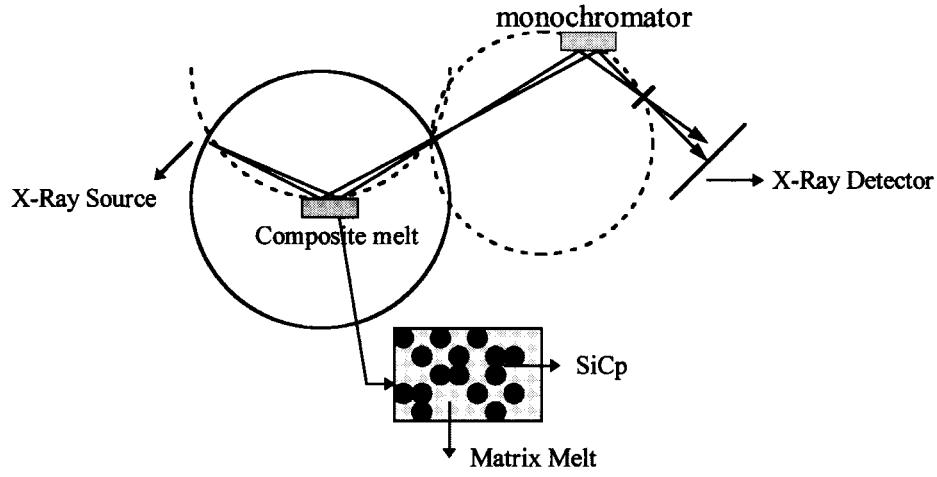

Figure 1 Schematic illustration of the liquid metal X-ray diffraction.

TABLE I Temperatures (°C) of the diffraction measurement with different composition

Pure Al	675	775	875	1075
10 vol % SiCp/Al	675	775	875	1075
40 vol % SiCp/Al	675	775	875	1075

of Science. Fig. 1 shows the schematic illustration of the liquid metal X-ray diffraction for SiCp/Al composites. MoK$_\alpha$ radiation (wavelength $\lambda = 0.07089$ nm), allowing data to be taken from $Q \sim 10$ nm^{-1} to $Q \sim 120$ nm^{-1}, is reflected from the free surface of the specimen, reaches the detector though a graphite monochromator in the diffraction beam. High temperature X-ray diffractions were carried out in a high purity helium atmosphere of 1.3×10^5 Pa before the chamber was cleaned in vacuum of 2×10^{-6} Pa. Specimens were placed in an alumina crucible of $30 \times 25 \times 8$ mm in size, using a Ta sheet as heating element, and the surface of the specimen was fixed to one horizontal position using a laser calibrator. Some other parameters used in this experiment included: scanning voltage 40 kV, current was 30 mA, exposure time 30 s, measured angle 2θ was from 5–90 deg. The experimental temperature and composition of the material were listed in Table I.

2.3. Data processing for liquid structure

The information on the structure of composite melt was obtained after the solid phase information was filtered from the diffraction intensity profiles [7]. The details of the data processing for the liquid melt can also be seen in [8]. The following is an outline of the processing.

The scattering intensity measured in arbitrary units can be converted into the coherent scattering intensity per atom in an electron unit I_a^{coh}, using the generalized Krogh–Moe–Norman method. Compton scattering is also corrected using the values reported by Cromer and Mann. Multiple scanning, resulting in an accumulation of more than 3×10^4 counts per angle, reducing the total estimate of error for the structure factor $S(Q)$, to less than ±2%. The total structure factor can be written as

$$S(Q) = \frac{I_a^{coh}}{\langle f^2(Q)\rangle} = c_1k_1^2S_{11}(Q) + c_2k_2S_{22}(Q) + 2(c_1c_2)^{1/2}k_1k_2S_{12}(Q) \quad (2)$$

in Equation 2, the partial structure factors

$$S_{ij}(Q) = \delta_{ij} + \int_0^o 4\pi r^2[\rho_{ij}(r) - c_j\rho_0]\frac{\sin(Qr)}{Qr}\,dr \quad (3)$$

The pair distribution function $g(r)$ was a Fourier transformation of the structure factor $S(Q)$ deduced from I_a^{coh}:

$$g(r) = 1 + \frac{1}{2\pi^2\rho_0 r}\int_0^o Q[S(Q) - 1]\sin(Qr)\,dQ \quad (4)$$

where Q is the scattering vector, $Q = \frac{4\pi\sin(\theta)}{\lambda}$, 2θ is the scattering angle, λ is the wavelength of the diffraction beam, $c_i = N_i/N$, and c_i, N_i are concentration and number of atom type i in the melt, N is the total number in the scattering volume, $k_i = \frac{f_i}{[f^2(Q)]^{1/2}}$, $[f^2(Q)] = \sum_i c_i f_i^2 f_i$ is the atomic scattering factor of atom type i, In addition, ρ_0 and r, are the average number density of atoms and the distance from the reference atom, respectively.

The size of short-range-order (SRO) in the liquid melt $r_c = g(\pm 1.02)$, representing the lower limit of the atom cluster [9].

2.4. Calorimetric measurements

The composite samples after the thermal history in liquid metal X-ray diffraction were remelted in a high purity alumina pan in a Netsch DSC404 instrument. Runs were carried out at a heating rate 20 °C min^{-1} from ambient to 850 °C, subsequently cooling to ambient temperature at 20 °C min^{-1}, and under dynamic high purity argon atmosphere (80 ml min^{-1}). High purity corundum was used as a reference, and all DSC thermograms were normalized to the actual amount of metal (in weight percent) in each composite.

3. Results of liquid metal X-ray diffraction

3.1. The structure factor and pair distribution function of the SiCp/Al composites melt

It is generally noted that the melting of the measured sample is not a simple process, but one that is rather time, temperature and composition dependent. The temperature variation of the structure factor $S(Q)$ and the distribution function $g(r)$ of melts are given in Figs 2 to 4 using the results of molten pure Al and SiCp/Al composite with 10% and 40 vol % reinforcement volume. The effect of increasing temperature on $S(Q)$ and $g(r)$ is, in general, to decrease the amplitude of the oscillating behavior, rather than to change the

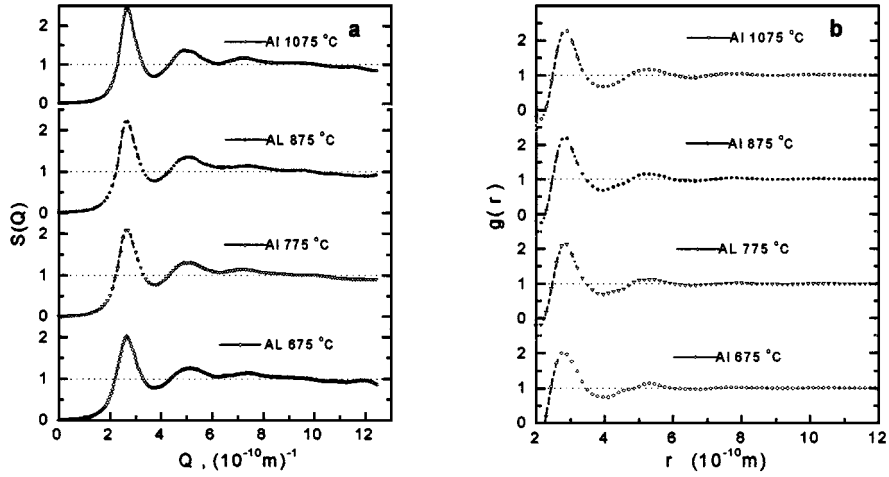

Figure 2 Temperature dependence of the structure factor $S(Q)$ and pair distribution function $g(r)$ for pure Al melt (a) $S(Q)$ and (b) $g(r)$.

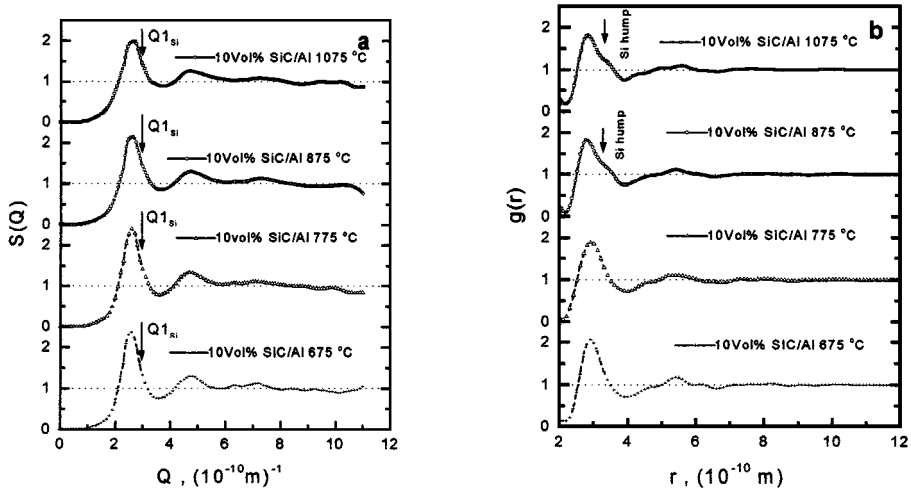

Figure 3 Temperature dependence of the structure factor $S(Q)$ and pair distribution function $g(r)$ for 10 vol %SiC/Al melt (a) $S(Q)$ and (b) $g(r)$.

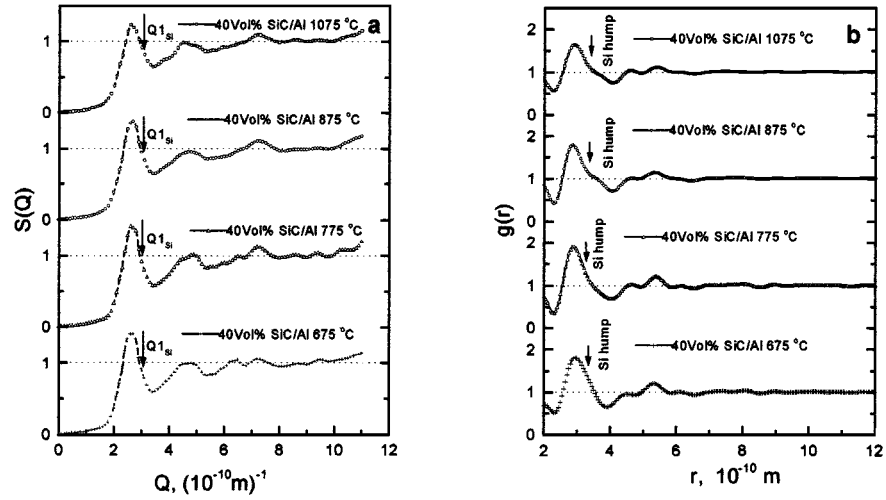

Figure 4 Temperature dependence of the structure factor $S(Q)$ and pair distribution function $g(r)$ for 40 vol %SiC/Al melt (a) $S(Q)$ and (b) $g(r)$.

position of the peaks. The temperature effect on the structure certainly depends on the melt composition.

Even though the data for the liquid Al and the SiCp/Al composite melt were measured at the same temperature, some differences are still demonstrated in structure factor $S(Q)$ and pair distribution function $g(r)$. As shown in Fig. 2, the melt of pure Al produced a very similar structure factor $S(Q)$ and pair distribution function $g(r)$ at different temperatures. All the results for the liquid Al maintain the same general features in the structure factor profiles. Namely, they all show a relatively sharp first peak and subsequent small peaks on the high Q region. This implies that the fundamental feature in atomic distributions for a liquid melt are approximated more or less by a random mixture. But the structure of SiCp/Al melt, as shown in Figs 3 and 4, is different from that of liquid pure Al, with the temperature increasing, the first peak of the $S(Q)$ curve becomes broader and more asymmetric, while the $g(r)$ is characterized by splitting of the second main peak into a large peak and two small ones, implying the melt is not well distributed [10].

It is immediately evident from Figs 3 and 4 that a small Si–Si hump [11] in the first main peak of $g(r)$ was observed, with increasing temperature. For 10 vol % SiCp/Al composite melt, the hump peak progressively emerged while holding at 875 °C, while it is very clear at 1075 °C. For 40 vol %SiCp/Al composite melt, the hump peak always exists in the first main peak of the $g(r)$ above 775 °C, the position of this hump is 0.32 nm or so.

3.2. The size of short-rang-order in SiCp/Al composite melt above the liquidus

Fig. 5 shows the temperature dependence of the size of short-range-order (SRO) in liquid Al and the two kinds of SiCp/Al composite melt, the size of SRO r_c in liquid Al reduces with increasing temperature, agreeing with the feature in the $g(r)$ of the liquid Al (see also Fig. 2b), implying that the fundamental features in the atomic distribution for the liquid are approximated more or less by a random mixture, whereas the size of SRO in SiCp/Al composite melt are reduced only above a given temperature, while it is more or less a constant, indicating the melt structure in SiCp/Al is different from that in liquid Al.

4. Discussion

4.1. The distribution of Si from the interfacial reaction

The Si–Si hump is the main characteristic feature of hypereutectic Al-Si with super high Si content [12], but our DSC study shown in Fig. 6 showed that SiCp/Al composite did not emerge as a feature of hypereutectic Al-Si melt after the thermal history in liquid metal X-ray diffraction and subsequent remelting. As illustrated in Fig. 6, for each kind of composite, the comparison of onset and end temperature of the Al-Si eutectic reaction and the changed liquidus temperature in the DSC heating and cooling trace suggested that the mean melt composition of the two kinds of SiCp/Al composites lies in the Al-Si hypoeutectic field. Both

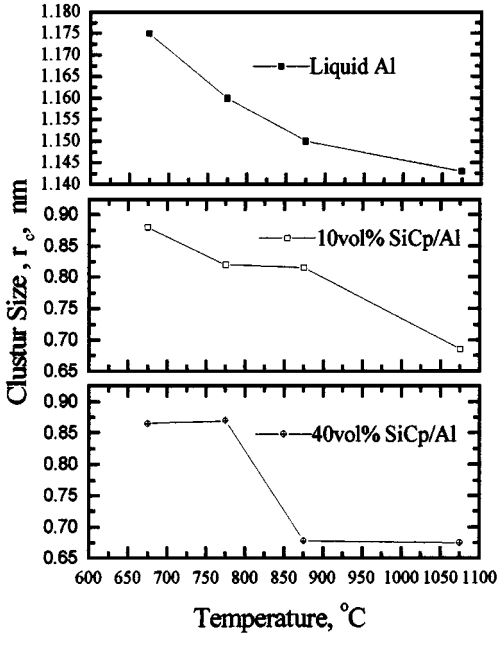

Figure 5 Temperature dependence of cluster size in liquid Al and SiCp/Al composite melt.

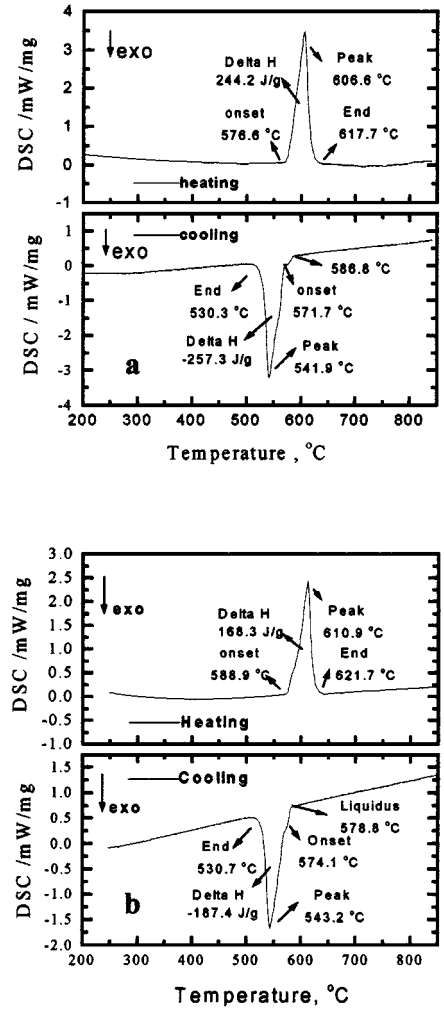

Figure 6 DSC trace for the remelting of SiCp/Al composites (a) 10 vol % and (b) 40 vol %.

results suggest that in the SiCp/Al composite melt a solute-rich region with much more Si content exists.

4.2. The diffusion of Si above the liquidus

It is well known that the liquid metal is characterized by short-range-order and the cluster size r_c is the lower limit of the atom cluster, from the standpoint of the hard-sphere model in liquid metal structure theory [13], r_c is associated with the packing density η of the atom cluster, which is defined by $\eta = (\pi/6)n_0\sigma^3$, where σ is atom diameter, the temperature dependence of packing density is expressed, in the first order approximation, by the following exponential function:

$$\eta(T) = A\exp(-QT) \tag{5}$$

where T is absolute temperature, the parameter A, based on experimental data for various metals, is a constant, Q is the diffusion active energy. As seen in Equation 5 as the temperature T increases, the packing density η decreases, so the size of SRO r_c is small, but not linear. The size change in liquid Al implied that the fundamental features in the atomic distribution for the liquid are approximated, more or less by a random mixture, and agreed with the above equation. In SiCp/Al composite melt, according to Equation 1, with temperature increasing, $Al + SiC \rightarrow [Al\text{-}Si] + Al_4C_3 + SiC$, liquid Al is progressively becoming liquid Al-Si, and the theoretical calculation results showed that in Al-Si melt, the SRO is mainly Si–Si cluster [14], because the bond energy on Si–Si pairs is the strongest among Al–Al, Al–Si and Si–Si pairs. The size change of SRO in SiCp/Al composite melt suggested that the diffusion of Si from the chemical reaction between SiC and molten Al can diffuse only after a given temperature or the concentration fluctuation of Si.

4.3. The nature of the distribution and diffusion of Si above the liquidus

The emergence of Si–Si humps and the size change of SRO are attributed to the chemical reaction between SiC and the melt and the variation of the viscosity in the composite melt. It is well known that molten metals and alloys are Newtonian fluids, viscosity is independent of shear rate and decreases with increasing temperature following the Arrhenius relation. When solid particles are dispersed in a liquid metal, two types of interaction can occur: a hydrodynamic interaction between liquid and the particles, and a non-hydrodynamic interaction between the particles themselves [15, 16]. Both interactions produce an increase in the apparent viscosity of the composite melt, these show that the apparent viscosity of various composite slurries are significantly higher than the unreinforced matrix alloy, often by orders of magnitude; on the other hand, additional variations in apparent viscosity may result from chemical reaction between the reinforcement and the matrix which alter the shape and volume fraction of the reinforcement. This effect has been shown to increase the apparent viscosity of Al-SiC particulate slurries [17, 18], at 750 °C, the spiral fluidity remains about constant with holding time, however, at 800 °C, resulting in a marked decrease in fluidity until, after 250 min, the composite will not flow. This is because SiC particles are relatively stable in Al-7Si below 750 °C, while they react at high temperature. Because the reactivity between SiC and pure Al is high, the effect of the chemical reaction upon the viscosity in SiCp/pure Al is much more than that in SiC/Al-7Si.

For a particle (atom or molecular) with radius r_i, the relationship between the diffusion coefficient and the viscosity of the melt agrees with the Stockes–Einstein equation [19]:

$$D_i = \frac{k_B T}{6\pi r_i \nu} \tag{6}$$

Where D_i represents the diffusion coefficient, ν represents viscosity of the melt, and k_B is the Boltzman constant, T is the absolute temperature. As seen in Equation 6, when ν becomes larger, the diffusion coefficient D_i is reduced, so the diffusion of atom i is more difficult. In fact, the effect of temperature change is more complex. In conventional liquid alloys, the viscosity decreases with increasing melt temperature, whereas the viscosity in SiC/Al composite decreases with increasing temperature and increasing SiC particle volume fraction due to the formation of Al_4C_3.

The decrease of apparent viscosity results in the difficulties of atom (Si and Al) diffusion and heat convection, thus impeding the solute Si, Al from the chemical reaction redistribution, with increasing temperature, the chemical reaction is more serious, the apparent viscosity is higher, Si from the chemical reaction is accumulated in local zones around the SiC particles, with an emerging Si–Si hump in the radial distribution function $g(r)$. As discussed above, only after a given temperature or a degree of concentration fluctuation of Si, is the diffusion of Si possible.

5. Conclusion

In the present work, liquid metal X-ray diffraction and DSC have been used to investigate the melt structure of SiCp/Al composite, the following results were obtained:

(1) A Si–Si hump emerging in the pair radial distribution function suggested that a Si-rich region exists in the SiC/Al composite melt above the liquidus, implying the Si is not well distributed above the liquidus;

(2) The size change of SRO in SiCp/Al composite indicated that the diffusion of Si from the chemical reaction between SiC and molten Al is possible only after a given temperature or a degree of concentration fluctuation of Si;

(3) The existence of the Si–Si hump and the size change of SRO are attributed to the chemical reaction in the SiCp/Al composite and the existence of reinforcing particles, high volume fraction has a greater influence on the Si–Si hump and the size change of SRO than the low volume fraction.

Acknowledgement

The authors are grateful for the finance support of the National Nature Science Foundation of People's Republic of China under grant No. 59 631 080.

References

1. W. H. YOUNG, *Rep. Prog. Phys.* **55** (1992) 1769.
2. U. BALUCANI, A. TOREINI and R. VALLAURI, *Phys. Rev. B* **47** (1993) 3011.
3. ZHUANG H. Z., ZOU X. W. and JIN Z. Z., *ibid.* **52** (1995) 829.
4. V. M. BERMUDEZ, *Appl. Phys. Lett.* **42** (1983) 70.
5. L. PORTE, *J. Appl. Phys.* **60** (1986) 635.
6. K. KANNIKESWARAN and R. Y. LIN, *J. Met.* **39** (1987) 17.
7. Y. TSUCHIYA, S. TAMAKI and Y. WASEDA, *J. Phys. C.* **12** (1979) 5361.
8. Y. WASEDA. *Prog. Mater. Sci.* **26** (1981) 1.
9. V. V. BUHALENKO, A. G. ILINKII and A. V. ROMANOVA et al. *Metallofizika* **13** (1991) 92.
10. H. S. CHEN and WASEDA. *Phys. Status Solids. A,* **51** (1979) 593.
11. Y. KITA, J. B. VANZYTVELD and Z. MORITA. *J. Phys. Condens Matter*, **6** (1994) 811.
12. J.-P. GABATHULER, S. STEEB and P. LAMPARTER. *Z. Nat. forsch. A,* **34** (1979) 1305.
13. J. D. BERNAL, *Nature* **185** (1960) 68.
14. LI-P. J., CHENG-G. and YU-R. H. *Acta Sci. Natur. Univ. Jilinesis.* **3** (1997) 61.
15. G. K. BATCHLOR, *Annu. Rev. Fluid. Mech.* **6** (1974) 227.
16. R. HERBZYNSKI and I. PIENKOWSKA, *Annu. Rev. Fluid. Mech.* **12** (1980) 237.
17. D. J. LLOYD, *Compos. Sci. Technol.* **35** (1989) 159.
18. A. MORTENSEN and I. JIN, *Int. Mater. Rev.* **37** (1992) 101.
19. A. EINSTEIN, *Z. Electrochem.* **17** (1908) 1908.

Received 18 June
and accepted 21 July 1998